

Machine learning effective models for quantum systems

Jonas B. Rigo and Andrew K. Mitchell

School of Physics, University College Dublin, Belfield, Dublin 4, Ireland

The construction of good effective models is an essential part of understanding and simulating complex systems in many areas of science. It is a particular challenge for correlated many body quantum systems displaying emergent physics. We propose a machine learning approach that optimizes an effective model based on an estimation of its partition function. The success of the method is demonstrated by application to the single impurity Anderson model and double quantum dots, where non-perturbative results are obtained for the old problem of mapping to effective Kondo models. For quantum impurity parent Hamiltonians, we derive an alternative approach based on learning from observables. When mapping to minimal effective models, emergent scales may not be captured by observable learning, while partition function learning may not reproduce all observables.

The approach to understanding and simulating complex quantum systems can be divided into two groups: *ab initio* studies in which one tries to account for all microscopic details, or studies of simplified effective models that still capture the essential physical phenomena of interest. A prerequisite for the latter is to construct a good effective model. The question of how to do this systematically, starting from a more complex microscopic system, is an important one for many areas of physics.

Effective models are often defined in a reduced Hilbert space involving only those degrees of freedom relevant to describe the low-temperature physics of a complex microscopic model. They can be derived by perturbatively eliminating degrees of freedom, coarse-graining, or by using renormalization group (RG) methods [1–4]: at low energies, microscopic details only enter through effective interactions and renormalized coupling constants. For the purposes of simulation, and to make realistic contact with experiment, the parameters as well as the structure of an effective model must be determined.

In this Letter, we use information theory and machine learning (ML) methods to find good effective models for quantum many-body systems. We devise two different approaches. The first is based on comparing the low-energy eigenspectrum of the effective and microscopic models (see Fig. 1), which gives a simple optimization condition on their partition functions (‘model ML’). The second approach compares the distribution of diagrams in a perturbative expansion, yielding an optimization condition on local observables. The two methods only agree at the Gibbs-Bogoliubov-Feynman [5] (GBF) bound. For *minimal* effective models comprising only RG-relevant terms, learning from observables may not yield the same effective model parameters compared with learning from the partition function, since observables can flow under RG while the partition function does not [1, 2, 6]. The correct low-energy physics is obtained when the partition functions of bare and effective models agree. Minimally-constrained effective models may be able to reproduce the same low-energy physics and the same observables as the parent Hamiltonian. Applications of ML optimization using observables have been discussed in Refs. [7–9].

Effective models are also used in self-learning Monte Carlo [8–11]. ML is used to optimize effective Hamiltonians that can be treated more efficiently while reproducing the same Monte Carlo update weights as the bare Hamiltonian for sampled configurations. Such methods are not straightforwardly applicable to systems where the effective model involves rather different degrees of freedom, or the emergent physics is non-perturbative.

The full potential for applying ML concepts in physics is still being explored. Intense recent activity in the field covers a diverse range of topics, including: (i) finding and describing eigenstates [12–18]; (ii) the inverse problem of finding parent Hamiltonians [19–22]; (iii) predicting properties of materials [23–25]; (iv) identifying phases of matter [26–33]; (v) improving numerical simulations [8–11, 34–40]; (vi) connections between ML and RG [41–46].

Concepts from physics are also often used in ML algorithms [47–49] – perhaps most notably in Boltzmann machines [50, 51] where an unknown probability distribution is approximated by the physical Boltzmann weights of an auxiliary energy-based model. However, ML is gen-

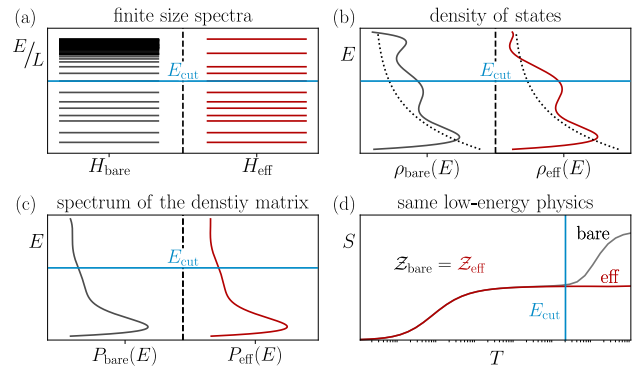


Figure 1. Schematic comparison of bare [left] and effective [right] models: (a) Finite size spectra, which agree up to some high-energy cutoff, E_{cut} . (b) Density of states (Boltzmann weighting $e^{-\beta E}$ as dotted line). (c) Spectrum of the thermal density matrix. (d) Thermodynamics, such as entropy, match at low temperatures $T \ll E_{\text{cut}}$ when $Z_{\text{eff}} = Z_{\text{bare}}$.

erally treated as a ‘black box’ method, since these models are typically of high complexity and abstraction with no physical meaning [52]. The methodologies described in this Letter constitute generative ML because samples from a target distribution (e.g. state diagrams [53]) are used to train a model that can generalize from those to generate new samples. Here, though, the auxiliary model is the actual low-energy effective model of interest, and has physical meaning. Importantly, we show that the mapping can be achieved at relatively high temperatures, without having to completely solve the bare Hamiltonian. *Partition function condition on effective models.*— As illustrated in Fig. 1, the goal is to find an effective model with the same low-energy eigenspectrum, or density of states $\rho(\omega)$, as the bare model. Since the effective model lives in a restricted Hilbert space, its high-energy spectrum is typically more sparse than the bare model. The regime of applicability of the effective model is therefore restricted below some cutoff E_{cut} . At low temperatures $T \ll E_{\text{cut}}$, the thermally-weighted density of states (density matrix spectrum) $q(\omega) = \exp(-\beta\omega)\rho(\omega)$ should therefore agree. This guarantees that the bare and effective models have the same low-temperature thermodynamics, including the same emergent energy scales. Note that if $q_{\text{bare}}(\omega) \simeq q_{\text{eff}}(\omega)$ at a given temperature, then the partition functions $\mathcal{Z} = \int d\omega q(\omega)$ necessarily match.

In principle, optimizing an effective model could be achieved by minimizing the difference between the bare and effective probability distributions $P(\omega) = q(\omega)/\mathcal{Z}$ by minimizing their Kullback-Leibler (KL) divergence [54],

$$D_{\text{KL}} = \int d\omega P_{\text{eff}}(\omega) \log[P_{\text{eff}}(\omega)/P_{\text{bare}}(\omega)] . \quad (1)$$

ML algorithms based in this way on optimizing with respect to the density matrix are referred to as ‘quantum Boltzmann machines’ [49]. The problem is that this rigorous prescription only applies in the eigenbasis of the models, and the gradient descent update required to find the optimal effective model involves taking derivatives of Eq. 1 with respect to tuning parameters. In most cases this is not practicable, and the ML algorithm itself would need to be run on a quantum computer [47].

Our central result is that this can be avoided if we restrict our attention to effective models that can *in principle* be derived by a continuous RG transformation from the bare/microscopic model. In particular, the low-energy spectrum of the effective model should remain in one-to-one correspondence with the bare model, with the same quantum numbers, and the symmetries of the bare model are preserved (although the effective model may have larger symmetries). We exclude, for example, a large class of effective models involving a non-interacting quantum gas fine-tuned to trivially reproduce the desired eigenspectrum, or other unphysical models. While an RG-derivable effective model $\hat{H}_{\text{eff}} = \sum_i \theta_i \hat{h}_i$ may have high physical complexity, its parametric com-

plexity $\{\theta_i\}$ is typically modest. A given effective model has correspondingly modest expressibility in terms of describing different physical systems; the structure of an effective model must be appropriate to the physics being described. This is unlike the standard philosophy for Boltzmann machines that employ an unphysical auxiliary energy-based model to represent $P_{\text{bare}}(\omega)$, with high expressibility but also high parametric complexity [50].

Since the RG process can be regarded as a ‘quantum channel’ [6] (a completely positive, trace preserving linear map [55]), the partition function is invariant under RG [1]. An RG-derivable effective model therefore satisfies the condition, $\mathcal{Z}_{\text{eff}} = \mathcal{Z}_{\text{bare}}$. Optimization can therefore be done directly on the level of the partition functions.

Our model ML does not perform RG: given a suitable structure for the effective model, the method finds the optimized model parameters by matching partition functions. Even though the partition function is a single number, the method works because we use prior knowledge to restrict the search space. With loss function $L_{\mathcal{Z}} = [\log(\mathcal{Z}_{\text{eff}}) - \log(\mathcal{Z}_{\text{bare}})]^2$, the gradient descent update for tuning a parameter θ_i of the effective model is

$$\partial L_{\mathcal{Z}} / \partial \theta_i \sim [\log(\mathcal{Z}_{\text{eff}}) - \log(\mathcal{Z}_{\text{bare}})] \times \langle \hat{h}_i \rangle_{\text{eff}} . \quad (2)$$

The partition functions themselves can be estimated by any suitable method at any temperature $T < E_{\text{cut}}$.

Model machine learning for the Anderson model.— As a simple but non-trivial demonstration, we apply the model ML scheme to the Anderson impurity model (AIM) [56],

$$\hat{H}_{\text{A}} = \hat{H}_{\text{bath}} + \sum_{\sigma} \epsilon \hat{n}_{d\sigma} + U \hat{n}_{d\uparrow} \hat{n}_{d\downarrow} + V \sum_{\sigma} (d_{\sigma}^{\dagger} c_{0\sigma} + c_{0\sigma}^{\dagger} d_{\sigma}) \quad (3)$$

where $\hat{H}_{\text{bath}} = \sum_{k,\sigma} \epsilon_k c_{k\sigma}^{\dagger} c_{k\sigma}$, $\hat{n}_{d\sigma} = d_{\sigma}^{\dagger} d_{\sigma}$, and $V c_{0\sigma} = \sum_k V_k c_{k\sigma}$. For simplicity we consider particle-hole symmetry $\epsilon = -U/2$, and a flat conduction electron density of states in a band of half-width $D = 1$.

The Kondo Hamiltonian is the low-energy effective model [56, 57], describing impurity-mediated scattering,

$$\hat{H}_{\text{K}} = \hat{H}_{\text{bath}} + J \hat{S}_d \cdot \hat{S}_0 , \quad (4)$$

where \hat{S}_d is a spin- $\frac{1}{2}$ operator for the impurity, and $\hat{S}_0 = \frac{1}{2} \sum_{\sigma,\sigma'} \vec{\tau}_{\sigma\sigma'} c_{0\sigma}^{\dagger} c_{0\sigma'}$ is the spin density of conduction electrons at the impurity. For generality, we specify the Kondo conduction electron bandwidth as D_{K} . For a pure Kondo model, Eq. 4, the Kondo temperature determining the low-energy physics is given by [58, 59],

$$T_{\text{K}}(J, D_{\text{K}}) = \alpha D_{\text{K}} \sqrt{\rho J} \exp[-1/\rho J + \gamma \rho J] , \quad (5)$$

where $\rho = 1/2D_{\text{K}}$ is the Fermi level free density of states, $\gamma = \pi^2/4$, and $\alpha = \mathcal{O}(1)$ [59].

The Kondo model is the minimal model consistent with bare symmetries of the AIM (we do not consider minimally-constrained effective models, and retain only

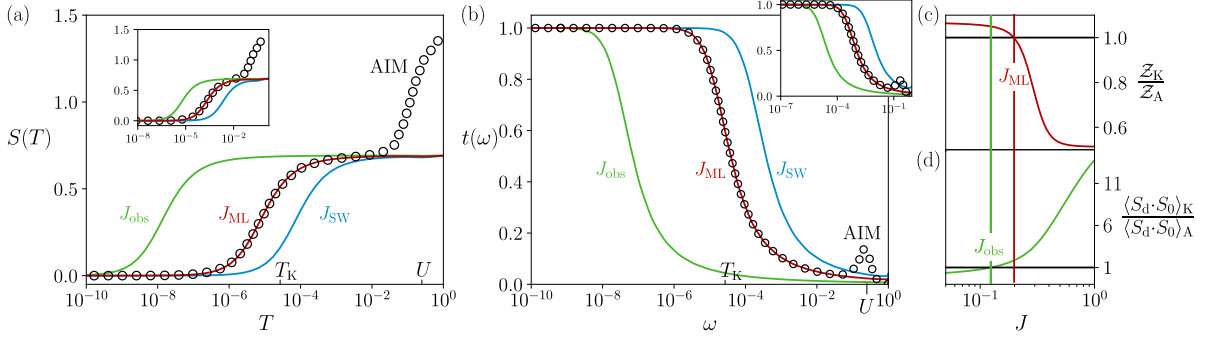


Figure 2. Model ML derivation of the Kondo model from the Anderson impurity model. (a) Impurity contribution to entropy, $S(T)$; (b) $T = 0$ spectrum of the t-matrix, $t(\omega)$. AIM results for $U = 0.5$ and $8V^2/U = 0.25$ shown as circle points. Lines are for Kondo models with $J = J_{\text{ML}}$ optimized by model ML (red lines), J_{obs} obtained by observable matching (green lines), and J_{SW} for Schrieffer-Wolff (blue lines). Insets show the same but for reference AIM with $8V^2/U = 0.4$. (c) Ratio of partition functions $\mathcal{Z}_K/\mathcal{Z}_A$ for the model ML optimized Kondo model and the reference AIM; (d) corresponding ratio of spin-spin correlators.

RG-relevant terms [57]). Traditionally, the Kondo model is derived from the AIM by the Schrieffer-Wolff (SW) transformation [3], which perturbatively eliminates excitations out of the singly-occupied impurity manifold. SW yields $J_{\text{SW}} = 8V^2/U$ to second order in the impurity-bath hybridization. More sophisticated methods are required to capture non-perturbative renormalization effects neglected by pure SW [57, 60–62]. The full solution of both Anderson and Kondo models enables comparison of T_K [57, 61]; the results are often interpreted in terms of a renormalized Kondo bandwidth, $D_K \rightarrow D_{\text{eff}} \leq D$.

Here we use the numerical renormalization group (NRG) method [4, 59, 63] to determine the partition functions of the Anderson and Kondo models (\mathcal{Z}_A and \mathcal{Z}_K respectively) at temperature T . We optimize the Kondo coupling J by minimizing L_Z using bisection. NRG results are presented in Fig. 2, comparing the bare AIM (circle points) with effective Kondo models ($D_K = D = 1$): J determined by model ML (red lines), the SW result $J_{\text{SW}} = 8V^2/U$ (blue lines), and J obtained by observable matching (green lines, discussed shortly). Panel (a) shows the impurity contribution to entropy $S(T)$, for $U = 0.5$ and $J_{\text{SW}} = 0.25$ (inset for $U = 0.5$ and $J_{\text{SW}} = 0.4$), while panel (b) shows the scattering t-matrix spectrum $t(\omega)$, at $T = 0$ for the same parameters. Panels (c,d) show the ML optimization procedure.

Figs. 2(a,b) demonstrate that the model ML method perfectly determines the true coupling J of the effective Kondo model – even in the case where an incipient local moment is never fully developed (insets). By contrast, the pure SW result substantially over-estimates the coupling, leading to the wrong low-energy physics and Kondo scales. In more complex models, errors in determining the couplings may lead to incorrect ground state assignment. Deviations between the AIM and Kondo model with $J = J_{\text{ML}}$ set in only at high temperature scales $T \sim U$ (impurity charge fluctuations in the AIM cannot

be described by the Kondo model [56]).

In the AIM and Kondo models, the density of states $\rho(\omega) = -\frac{1}{\pi} \sum_k \text{Im} G_{kk}(\omega)$, is related to the t-matrix via $G_{kk'}(\omega) = G_{kk'}^0(\omega) + G_{kk'}^0(\omega) t_{kk'}(\omega) G_{k'k'}^0(\omega)$, where $G_{kk'}$ and $G_{kk'}^0$ are the full and free electron Green’s functions [56]. All non-trivial correlations are encoded in the t-matrix spectrum $t(\omega)$ [59] plotted in Fig. 2(b). Matching the low-energy density of states as per Fig. 1(b) is therefore equivalent to matching the low-energy t-matrix. However, we have shown that this is achieved automatically by satisfying the simpler condition $\mathcal{Z}_K = \mathcal{Z}_A$.

Fig. 3(a) shows the evolution of the Kondo coupling J obtained by model ML for a reference AIM with fixed $J_{\text{SW}} = 0.3$, but varying U (red line). Panel (b) shows that the Kondo temperature $T_K(J_{\text{ML}}, D)$ of the ML-optimized Kondo model from Eq. 4 agrees perfectly with the true T_K^{AIM} of the AIM (circle points). The deviations from $T_K(J_{\text{SW}}, D)$ are clearly seen: only at very large $U \gg D$ does $T_K(J_{\text{ML}}, D) \rightarrow T_K(J_{\text{SW}}, D)$. We find [59]:

$$T_K^{\text{AIM}} \simeq T_K(J_{\text{SW}}, D) \times \frac{U}{U + 3.2D + 17.3J_{\text{SW}}}, \quad (6)$$

$$\equiv T_K(J_{\text{SW}}, D_{\text{eff}}), \quad (7)$$

where the Kondo bandwidth renormalization is $D_{\text{eff}}/D = T_K^{\text{AIM}}/T_K(J_{\text{SW}}, D)$, consistent with known asymptotes $D_{\text{eff}} \sim U$ for U and $\rho J \ll D$ [57, 60, 61], and recovering $D_{\text{eff}} \rightarrow 1$ for $U \gg D$ where pure SW suffices. Inverting Eq. 6 provides an accurate estimate of the true coupling J of the AIM in terms of the pure SW result.

Fig. 3(c) shows how the results of model ML depend on temperature. We perform optimization of the Kondo coupling J by matching partition functions at temperature T for three reference AIM with the same T_K but different U, V . We find that J_{ML} is robust and essentially constant for all $T \ll U$, where one expects the Kondo model to apply (in practice, J is obtained with less than 3% error for $U/T > 100$). This has the important

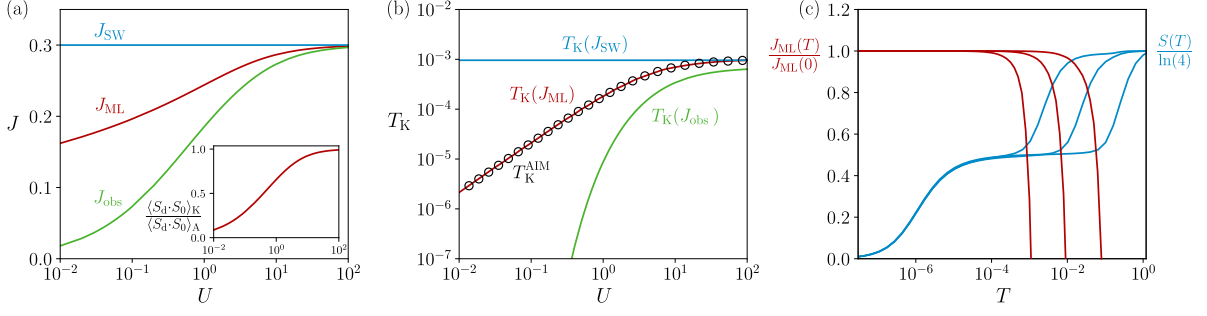


Figure 3. (a) Kondo coupling J optimized by model ML (red line) and observable matching (green line) for a reference AIM with fixed $8V^2/U = 0.3$, varying U . (b) Corresponding Kondo temperature T_K (circle points for the bare AIM). Inset to (a) shows ratio of spin-spin correlators in the model ML optimized Kondo model and the bare AIM. (c) Temperature-dependence of J obtained by model ML (red lines) for three AIMs with the same T_K but varying U, V [$S(T)$ also plotted for comparison].

implication that model ML can be performed using estimates of the partition functions at relatively high temperatures, making it amenable to treatment with e.g. quantum Monte Carlo methods [64–66]. Note that for $T \gtrsim U$, the Kondo model is not a good effective model, and the resulting J_{ML} vanishes as per Eq. 2.

A further application of model ML to double quantum dots is given in the Supplementary Material [59].

Optimization using observables.— ML employing heuristic cost functions based on physical observables might seem appealing if the goal is to reproduce observables of the bare model within the simpler description of an effective model. However, this is not always possible if one considers only *minimal* effective models. In general, a minimal model optimized to capture the proper low-energy physics cannot reproduce the value of all local observables in the bare model, even at low temperatures. This is due to information monotonicity along RG flow (the value of observables may flow under RG).

This result is presaged by the GBF inequality [5] for the free energy, $F_{\text{eff}} \leq F_{\text{bare}} + \langle \hat{H}_{\text{eff}} - \hat{H}_{\text{bare}} \rangle_{\text{bare}}$. Differentiating with respect to the coupling constants of the effective model $\hat{H}_{\text{eff}} = \sum_i \theta_i \hat{h}_i$, we obtain $\langle \hat{h}_i \rangle_{\text{eff}} \leq \langle \hat{h}_i \rangle_{\text{bare}}$. GBF implies that, when optimizing the effective model with respect to θ_i , the corresponding observable $\langle \hat{h}_i \rangle$ is merely *bounded* by its value in the bare model, not necessarily equal to it. ML using observables and ML involving the partition function only agree at the GBF bound.

In the case of mapping AIM to Kondo, we find that the proper effective model (J determined by model ML) yields $\langle \vec{S}_d \cdot \vec{S}_0 \rangle_K \leq \langle \vec{S}_d \cdot \vec{S}_0 \rangle_A$, with the GBF bound satisfied only in the limit $U \rightarrow \infty$, see inset to Fig. 3(a).

To compare with model ML, we implement optimization of the effective Kondo model using the observable-based cost function $L_J = [\langle \vec{S}_d \cdot \vec{S}_0 \rangle_K - \langle \vec{S}_d \cdot \vec{S}_0 \rangle_A]^2$. The green lines in Fig. 2 show the result of minimizing L_J . The Kondo model with $J = J_{\text{obs}}$ has the same impurity-bath spin correlation as the reference AIM, but does not yield the correct low-energy physics or Kondo scale (pan-

els a,b). Panels (c,d) show that $\langle \vec{S}_d \cdot \vec{S}_0 \rangle_K = \langle \vec{S}_d \cdot \vec{S}_0 \rangle_A$ and $\mathcal{Z}_K = \mathcal{Z}_A$ cannot be simultaneously satisfied. Fig. 3(a) shows how J_{obs} varies with U for fixed J_{SW} . Only for $U \rightarrow \infty$ does $J_{\text{obs}} \rightarrow J_{\text{ML}}$. For $U < 1$, J_{obs} is a poor approximation to the true J ($\simeq J_{\text{ML}}$), as highlighted by the differences in Kondo scales in panel (b).

ML based on diagrammatic expansion.— Finally, we derive rigorously an alternative ML approach using a classical probability distribution extracted from a diagrammatic expansion of the partition function, serving as a proxy for the Hamiltonian. We focus on generalized quantum-impurity problems $\hat{H} = \hat{H}_{\text{imp}} + \hat{H}_{\text{bath}} + \hat{H}_{\text{hyb}}$, of which AIM and Kondo are the simplest examples. The partition function may be written in terms of the continuous-time hybridization expansion [53, 60, 67], viz:

$$\mathcal{Z} = \mathcal{Z}_{\text{bath}} \int dx w(x), \quad (8)$$

$$w(x) = \det(\Delta^{(x)}) \Lambda^{(x)} \exp[-\beta \langle \hat{H}_{\text{imp}} \rangle_x], \quad (9)$$

where $w(x)$ is the weight of a distinct Feynman diagram labelled by the tuple x , $\Delta^{(x)}$ is the antiperiodic hybridization matrix, $\Lambda^{(x)}$ is a product of Dyson orbitals, and $\langle \hat{H}_{\text{imp}} \rangle_x$ is the expectation value of the impurity Hamiltonian on diagram x . Observables are evaluated as $\langle \hat{O} \rangle = \int dx w(x) \langle \hat{O} \rangle_x$. Further details and discussion are provided in the Supplementary Material [59].

For $w(x) > 0$, one may define a classical probability distribution of diagrams, $P(x) = (\mathcal{Z}_{\text{bath}}/\mathcal{Z})w(x)$. As with the classical Boltzmann machine, $P(x)$ is in the form of an energy-based model, with the weights here distributed according to the impurity Hamiltonian. The distribution of diagrams for bare and effective models can be compared using the KL divergence, Eq. 1. The parameters θ_i of the effective impurity Hamiltonian can be optimized by minimizing the KL divergence. The ML gradient descent update is $\nabla_{\theta} D_{\text{KL}}[P_{\text{eff}} : P_{\text{bare}}] = \beta \langle \nabla_{\theta} \hat{H}_{\text{eff}} \rangle_{\text{bare}} - \beta \langle \nabla_{\theta} \hat{H}_{\text{eff}} \rangle_{\text{eff}}$, provided $\nabla_{\theta} \Lambda_{\text{eff}}^{(x)} = 0$. This is a strictly convex optimization problem, with the minimum found when the impurity observables match.

This derivation reveals subtleties about the applicability of learning effective models from observables [59]. In particular, we highlight the fact that observable matching merely minimizes the KL divergence – it does *not* imply that $P_{\text{eff}}(x) = P_{\text{bare}}(x)$ or that $\mathcal{Z}_{\text{eff}} = \mathcal{Z}_{\text{bare}}$.

Conclusion and applications.– Finding a good effective low-energy model for a given bare Hamiltonian is a challenging and subtle problem. In this Letter we approach the problem using ML techniques, showing that optimization on the level of the partition function yields the correct low-energy physics for minimal RG-derivable effective models. However, not all local observables are necessarily reproducible in such a model. It remains an open question as to whether *minimally-constrained* effective models are able to capture simultaneously the universal low-energy physics as well as local observables.

The model ML framework we introduce is general; applications include deriving effective models for complex molecular junctions [68], and solving inverse problems for rational design. Model ML may also be adapted to find the effective equilibrium problem for non-equilibrium systems [69], or to find simplified/coarse-grained effective descriptions within multi-orbital/cluster dynamical-mean-field-theory [40, 70].

Acknowledgments.– We thank Sudeshna Sen for useful discussions, and acknowledge funding from the Irish Research Council Laureate Awards 2017/2018 through grant IRCLA/2017/169.

[1] J. L. Cardy, *Scaling and renormalization in statistical physics* (1996).
[2] K. G. Wilson, Phys. Rev. B **4**, 3174 (1971).
[3] J. R. Schrieffer and P. A. Wolff, Phys. Rev. **149**, 491 (1966).
[4] K. G. Wilson, Rev. Mod. Phys. **47**, 773 (1975); R. Bulla, T. A. Costi, and T. Pruschke, Rev. Mod. Phys. **80**, 395 (2008).
[5] R. Feynman, *Statistical Mechanics: A Set Of Lectures*, Advanced Books Classics (Avalon Publishing, 1998).
[6] C. Bény and T. J. Osborne, Phys. Rev. A **92**, 022330 (2015).
[7] K. Pakrouski, arXiv:1907.05898 (2019).
[8] J. Liu, Y. Qi, Z. Y. Meng, and L. Fu, Phys. Rev. B **95**, 041101 (2017).
[9] J. Liu, H. Shen, Y. Qi, Z. Y. Meng, and L. Fu, Phys. Rev. B **95**, 241104 (2017).
[10] Y. Nagai, H. Shen, Y. Qi, J. Liu, and L. Fu, Phys. Rev. B **96**, 161102 (2017).
[11] H. Shen, J. Liu, and L. Fu, Phys. Rev. B **97**, 205140 (2018).
[12] G. Carleo and M. Troyer, Science **355**, 602 (2017).
[13] A. Nagy and V. Savona, Phys. Rev. Lett. **122**, 250501 (2019).
[14] Z. Cai and J. Liu, Phys. Rev. B **97**, 035116 (2018).
[15] G. Carleo, K. Choo, D. Hofmann, J. E. T. Smith,

T. Westerhout, F. Alet, E. J. Davis, S. Efthymiou, I. Glasser, S.-H. Lin, M. Mauri, G. Mazzola, C. B. Mendl, E. van Nieuwenburg, O. O'Reilly, H. Theveniaut, G. Torlai, and A. Wietek, arXiv:1904.00031 (2019).
[16] I. Glasser, N. Pancotti, M. August, I. D. Rodriguez, and J. I. Cirac, Phys. Rev. X **8**, 011006 (2018).
[17] K. Choo, G. Carleo, N. Regnault, and T. Neupert, arXiv:1807.03325 (2018).
[18] G. Torlai and R. G. Melko, arXiv:1905.04312 (2019).
[19] N. Wiebe, C. Granade, C. Ferrie, and D. G. Cory, Phys. Rev. Lett. **112**, 190501 (2014).
[20] A. Valenti, E. van Nieuwenburg, S. Huber, and E. Greplova, Phys. Rev. Research **1**, 033092 (2019).
[21] E. Bairey, I. Arad, and N. H. Lindner, Phys. Rev. Lett. **122**, 020504 (2019).
[22] H. Fujita, Y. O. Nakagawa, S. Sugiura, and M. Oshikawa, Phys. Rev. B **97**, 075114 (2018).
[23] K. T. Butler, D. W. Davies, H. Cartwright, O. Isayev, and A. Walsh, Nature **559**, 547 (2018).
[24] J. Nelson and S. Sanvito, arXiv:1906.08534 (2019).
[25] R. Lot, F. Pellegrini, Y. Shaidu, and E. Kucukbenli, arXiv:1907.03055 (2019).
[26] J. Carrasquilla and R. G. Melko, Nature Physics **13**, 431 EP (2017).
[27] Y.-T. Hsu, X. Li, D.-L. Deng, and S. Das Sarma, Phys. Rev. Lett. **121**, 245701 (2018).
[28] Y. Zhang, A. Mesaros, K. Fujita, S. D. Edkins, M. H. Hamidian, K. Ch'ng, H. Eisaki, S. Uchida, J. C. S. Davis, E. Khatami, and E.-A. Kim, Nature **570**, 484 (2019).
[29] K. Ch'ng, J. Carrasquilla, R. G. Melko, and E. Khatami, Phys. Rev. X **7**, 031038 (2017).
[30] W. Rzadzowski, N. Defenu, S. Chiacchiera, A. Trombettoni, and G. Bighin, arXiv:1907.05417 (2019).
[31] L. Wang, Phys. Rev. B **94**, 195105 (2016).
[32] B. S. Rem, N. Käming, M. Tarnowski, L. Asteria, N. Fläschner, C. Becker, K. Sengstock, and C. Weitenberg, Nature Physics **15**, 917 (2019).
[33] Y.-T. Hsu, X. Li, D.-L. Deng, and S. Das Sarma, Phys. Rev. Lett. **121**, 245701 (2018).
[34] L.-F. m. c. Arsenault, A. Lopez-Bezanilla, O. A. von Lilienfeld, and A. J. Millis, Phys. Rev. B **90**, 155136 (2014).
[35] L. Huang and L. Wang, Phys. Rev. B **95**, 035105 (2017).
[36] L. Huang, Y.-f. Yang, and L. Wang, Phys. Rev. E **95**, 031301 (2017).
[37] J. Chen, S. Cheng, H. Xie, L. Wang, and T. Xiang, Phys. Rev. B **97**, 085104 (2018).
[38] J. C. Snyder, M. Rupp, K. Hansen, K.-R. Müller, and K. Burke, Phys. Rev. Lett. **108**, 253002 (2012).
[39] M. Rupp, A. Tkatchenko, K.-R. Müller, and O. A. von Lilienfeld, Phys. Rev. Lett. **108**, 058301 (2012).
[40] T. Song and H. Lee, Phys. Rev. B **100**, 045153 (2019).
[41] E. de Mello Koch, R. de Mello Koch, and L. Cheng, arXiv:1906.05212 (2017).
[42] P. Mehta and D. J. Schwab, arXiv:1410.3831 (2014).
[43] S.-H. Li and L. Wang, Phys. Rev. Lett. **121**, 260601 (2018).
[44] M. Koch-Janusz and Z. Ringel, Nature Physics **14**, 578 (2018).
[45] C. Bény and T. J. Osborne, New Journal of Physics **17**, 083005 (2015).
[46] S. Apenko, Physica A: Statistical Mechanics and its Applications **391**, 62 (2012).
[47] J. Biamonte, P. Wittek, N. Pancotti, P. Rebentrost,

- N. Wiebe, and S. Lloyd, *Nature* **549**, 195 (2017).
- [48] V. Dunjko, J. M. Taylor, and H. J. Briegel, *Phys. Rev. Lett.* **117**, 130501 (2016).
- [49] M. H. Amin, E. Andriyash, J. Rolfe, B. Kulchytskyy, and R. Melko, *Phys. Rev. X* **8**, 021050 (2018).
- [50] I. Goodfellow, Y. Bengio, and A. Courville, *Deep learning* (MIT Press, 2017).
- [51] C. M. Bishop, *Pattern Recognition and Machine Learning (Information Science and Statistics)* (Springer-Verlag, Berlin, Heidelberg, 2006).
- [52] F. Doshi-Velez and B. Kim, arXiv:1702.08608 (2017).
- [53] E. Gull, A. J. Millis, A. I. Lichtenstein, A. N. Rubtsov, M. Troyer, and P. Werner, *Rev. Mod. Phys.* **83**, 349 (2011).
- [54] S. Kullback and R. A. Leibler, *Ann. Math. Statist.* **22**, 79 (1951).
- [55] V. Vedral, M. B. Plenio, M. A. Rippin, and P. L. Knight, *Phys. Rev. Lett.* **78**, 2275 (1997).
- [56] A. C. Hewson, *The Kondo Problem to Heavy Fermions*, Cambridge Studies in Magnetism (Cambridge University Press, 1993).
- [57] H. Krishna-Murthy, J. Wilkins, and K. Wilson, *Physical Review B* **21**, 1003 (1980).
- [58] N. Andrei, K. Furuya, and J. H. Lowenstein, *Rev. Mod. Phys.* **55**, 331 (1983).
- [59] See Supplementary Material, which contains references [71, 72].
- [60] F. Haldane, *Physical Review Letters* **40**, 416 (1978); F. D. M. Haldane, *Journal of Physics C: Solid State Physics* **11**, 5015 (1978).
- [61] A. Tsvelick and P. Wiegmann, *Advances in Physics* **32**, 453 (1983).
- [62] S. K. Kehrein and A. Mielke, *Annals of Physics* **252**, 1 (1996).
- [63] F. B. Anders and A. Schiller, *Phys. Rev. Lett.* **95**, 196801 (2005); A. Weichselbaum and J. von Delft, *Phys. Rev. Lett.* **99**, 076402 (2007).
- [64] C. H. Bennett, *Journal of Computational Physics* **22**, 245 (1976).
- [65] W. von der Linden, *Physics Reports* **220**, 53 (1992).
- [66] A. N. Rubtsov, V. V. Savkin, and A. I. Lichtenstein, *Phys. Rev. B* **72**, 035122 (2005).
- [67] K. Haule, *Phys. Rev. B* **75**, 155113 (2007).
- [68] A. K. Mitchell, K. G. L. Pedersen, P. Hedegård, and J. Paaske, *Nature Communications* **8**, 15210 EP (2017), article.
- [69] A. Schiller and S. Hershfield, *Phys. Rev. B* **62**, R16271 (2000).
- [70] G. Kotliar, S. Y. Savrasov, K. Haule, V. S. Oudovenko, O. Parcollet, and C. A. Marianetti, *Rev. Mod. Phys.* **78**, 865 (2006); T. Maier, M. Jarrell, T. Pruschke, and M. H. Hettler, *Rev. Mod. Phys.* **77**, 1027 (2005).
- [71] R. Žitko and J. Bonča, *Phys. Rev. B* **74**, 045312 (2006).
- [72] A. K. Mitchell, M. R. Galpin, S. Wilson-Fletcher, D. E. Logan, and R. Bulla, *Phys. Rev. B* **89**, 121105 (2014); K. M. Stadler, A. K. Mitchell, J. von Delft, and A. Weichselbaum, *Phys. Rev. B* **93**, 235101 (2016).

Machine learning effective models for quantum systems: Supplementary Material

Jonas B. Rigo and Andrew K. Mitchell
School of Physics, University College Dublin, Belfield, Dublin 4, Ireland

DOUBLE QUANTUM DOT

As a further demonstration of the model ML method, we now consider the parallel double quantum dot (DQD) model illustrated in Fig. S1. The DQD Hamiltonian reads,

$$H_{\text{DQD}} = H_{\text{bath}} + \sum_{\alpha=1,2} (H_{\text{imp}}^{\alpha} + H_{\text{hyb}}^{\alpha}) , \quad (\text{S1a})$$

$$H_{\text{imp}}^{\alpha} = \sum_{\sigma} \epsilon \hat{n}_{\alpha\sigma} + U \hat{n}_{\alpha\uparrow} \hat{n}_{\alpha\downarrow} , \quad (\text{S1b})$$

$$H_{\text{hyb}}^{\alpha} = V \sum_{\sigma} (d_{\alpha\sigma}^{\dagger} c_{0\sigma} + c_{0\sigma}^{\dagger} d_{\alpha\sigma}) , \quad (\text{S1c})$$

where $\hat{n}_{\alpha\sigma} = d_{\alpha\sigma}^{\dagger} d_{\alpha\sigma}$ is the number operator for dot $\alpha = 1, 2$. The physics of the DQD is much richer than that of the single dot case, due to the interplay between Kondo physics and an emergent RKKY interaction between the dots, mediated by the conduction electrons [1]. No simple perturbative approach to this problem exists, making the DQD a more stringent test of the model ML methodology.

On the scale $T \sim U$, charge fluctuations on the dots are frozen out, and the DQD can be understood as two free spins- $\frac{1}{2}$. On a lower scale $T \sim J_{\text{RKKY}}$, the emergent ferromagnetic RKKY interaction between the dots favours a low-energy spin-1 DQD configuration. Finally, below the Kondo scale T_K , the collective DQD spin-1 state is Kondo underscreened to leave a residual spin- $\frac{1}{2}$ local moment and a singular Fermi liquid. The low-energy physics is therefore described by an effective spin-1 Kondo model [1] (Eq. 4 but with a spin-1 impurity operator). Applying model ML, we determine the effective J of this spin-1 Kondo model, which is seen in Fig. S1 to perfectly reproduce the correct low-temperature behavior of the entropy, including the correct Kondo scale T_K . The effective spin-1 Kondo model applies for $T \ll J_{\text{RKKY}} \sim 10^{-3}$, an emergent scale which can be read off from Fig. S1 as the temperature at which the entropy crosses over from $S = \ln(4)$ (two free spins- $\frac{1}{2}$) to $S = \ln(3)$ (free spin-1).

The inset shows the evolution of J_{ML} as a function of interaction strength U for fixed $J_{\text{SW}} = 8V^2/U = 0.2$. We find that Eqs. 5 and 6 again hold (but with $\gamma = \pi^2/2$).

Finally, we note that a DQD in the *serial* configuration, rather than in parallel as shown above, has a singlet rather than doublet ground state. Since the spin-1 Kondo model is no longer a good effective model, the model ML method yields $J_{\text{ML}} = 0$, signaling that a different effective model should be chosen.

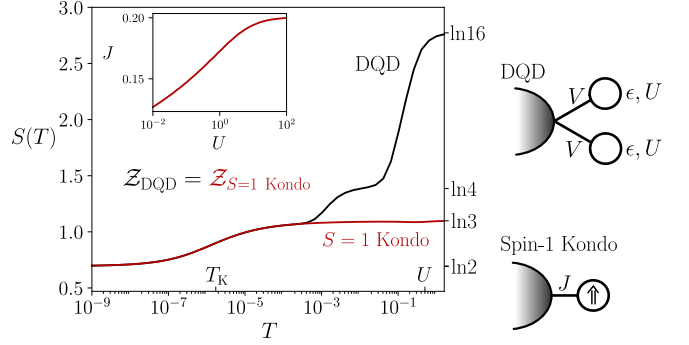


Figure S1. Impurity contribution to the entropy, $S(T)$, as a function of temperature, T , for the parallel double quantum dot model (Eq. S1) with $U = 0.5$ and $8V^2/U = 0.2$ (black line) compared with an effective spin-1 Kondo model with J determined by model ML (red line). Inset shows the evolution of J_{ML} with U for the same fixed $8V^2/U = 0.2$.

DETAILS OF ML BASED ON DIAGRAMMATIC EXPANSION

For a general Hamiltonian partitioned as $\hat{H} = \hat{H}_0 + \hat{H}_1$, one can compute the partition function as an expansion in powers of \hat{H}_1 by dividing into infinitesimal imaginary time slices [2],

$$\mathcal{Z} = \sum_{n=0}^{\infty} \frac{(-1)^n}{n!} T_{\tau} \int_0^{\beta} d\tau_1 \dots \int_0^{\beta} d\tau_n \times \text{tr} \left[e^{-\beta \hat{H}_0} \hat{H}_1(\tau_n) \dots \hat{H}_1(\tau_1) \right] . \quad (\text{S2})$$

This expansion is discussed extensively in the context of continuous time quantum Monte Carlo (CT-QMC) [3–5]. In the case of hybridization expansion CT-QMC [5] $\hat{H}_1 = \hat{H}_{\text{hyb}}$ describes the hybridization between a non-interacting bath \hat{H}_{bath} and an interacting quantum impurity \hat{H}_{imp} . For the following discussion, we therefore consider Hamiltonians of the form

$$\hat{H}_0 = \hat{H}_{\text{bath}} + \hat{H}_{\text{imp}} \quad (\text{S3a})$$

$$\hat{H}_1 = \hat{H}_{\text{hyb}} = \sum_k \sum_{\sigma} V_k^{\sigma} d_{\sigma}^{\dagger} c_{k\sigma} + \text{H.c.} , \quad (\text{S3b})$$

where we assume that the hybridization tensor is diagonal in the spin quantum number σ [5]. Eq. S2 can be interpreted as sum over all possible diagrams obtained by allowing electrons to hop between the impurity and the bath. Following the approach of Ref. [6], we bring

the impurity operators into the eigenbasis $\{(E_\alpha, |\alpha\rangle)\}$ of \hat{H}_{imp} and instead of occupation diagrams we obtain diagrams involving impurity eigenstates. This leaves us with a partition function in the form of Eq. 7,

$$\mathcal{Z} = \mathcal{Z}_{\text{bath}} \int dx w(x),$$

$$w(x) = \det(\Delta^{(x)}) \Lambda^{(x)} \exp[-\beta \langle \hat{H}_{\text{imp}} \rangle_x].$$

where $x = (n, \{k_i, k'_i, \sigma'_i, \sigma_i, \tau_i, \tau'_i\}_{i=1}^n)$ denotes a diagram in the eigenbasis [2]. Going from Eq. S2 to Eq. 7 we have integrated out the non-interacting bath and applied Wick's theorem to obtain the antiperiodic hybridization function

$$\begin{aligned} \det_{ij} [V_{k_i}^{\sigma_i} V_{k'_j}^{\sigma'_j*} \text{tr} (T_\tau e^{-\beta \hat{H}_{\text{bath}}} c_{k_i \sigma_i}^\dagger(\tau_i) c_{k'_j \sigma'_j}(\tau'_j))] \\ = \mathcal{Z}_{\text{bath}} \det_{ij} [V_{k_i}^{\sigma_i} V_{k'_j}^{\sigma'_j*} \langle T_\tau c_{k_i \sigma_i}^\dagger(\tau_i) c_{k'_j \sigma'_j}(\tau'_j) \rangle_{\text{bath}}] \\ = \mathcal{Z}_{\text{bath}} \det(\Delta^{(x)}). \end{aligned} \quad (\text{S5})$$

Bringing Eq. S2 into the eigenbasis has the effect that $e^{-\beta \hat{H}_{\text{imp}}}$ can be trivially evaluated, with

$$\beta \langle \hat{H}_{\text{imp}} \rangle_x = \sum_i^n [E_{\alpha_i}(\tau_i - \tau'_i) + E_{\alpha'_i}(\tau'_i - \tau_{i+1})], \quad (\text{S6})$$

where periodic boundary conditions $k+1 \rightarrow 1$ are implied. The transformation requires a projection of impurity operators onto the eigenbasis, viz

$$\Lambda^{(x)} = \prod_{i=1}^n \langle \alpha_i | d_{\sigma_i}^\dagger | \alpha'_i \rangle \langle \alpha'_i | d_{\sigma'_i} | \alpha_{i+1} \rangle. \quad (\text{S7})$$

The partition function now takes the form of Eq. 7.

From Eq. 7 we extract a classical probability distribution $P(x) = (\mathcal{Z}_{\text{bath}}/\mathcal{Z})w(x)$, provided $w(x) > 0$. This distribution acts as a proxy for the impurity Hamiltonian; to emphasize this dependency, we introduce the notation $P(\hat{H}_{\text{imp}}; x)$. This proxy can be used to compare two Hamiltonians. We write $P(\hat{H}_{\text{bare}}; x) = (\mathcal{Z}_{\text{bath}}/\mathcal{Z}_{\text{bare}})w_{\text{bare}}(x)$ for the bare model, and $P(\hat{H}_{\text{eff}}; x) = (\mathcal{Z}_{\text{bath}}/\mathcal{Z}_{\text{eff}})w_{\text{eff}}(x)$ for the effective model. The ‘distance’ between the bare and effective Hamiltonians can then be measured using the Kullback-Leibler divergence [7] of $P(\hat{H}_{\text{bare}}; x)$ and $P(\hat{H}_{\text{eff}}; x)$. From Eq. 1 we find,

$$\begin{aligned} D_{\text{KL}} [\hat{H}_{\text{bare}} : \hat{H}_{\text{eff}}] &= -\log(\mathcal{Z}_{\text{bare}}) + \log(\mathcal{Z}_{\text{eff}}) \\ &+ \int dx P(\hat{H}_{\text{bare}}; x) [\log |\Lambda_{\text{bare}}^{(x)}| - \log |\Lambda_{\text{eff}}^{(x)}|] \\ &- \beta \langle \hat{H}_{\text{bare}} \rangle_{\text{bare}} + \beta \langle \hat{H}_{\text{eff}} \rangle_{\text{bare}}, \end{aligned} \quad (\text{S8})$$

where we have used $\langle \hat{O} \rangle_{\text{bare}} = \int dx w_{\text{bare}}(x) \langle \hat{O} \rangle_x$ and $\langle \hat{O} \rangle_{\text{eff}} = \int dx w_{\text{eff}}(x) \langle \hat{O} \rangle_x$. In order to minimize this distance we use a gradient descent (GD) method, for which

we require the gradient of Eq. S8,

$$\begin{aligned} \nabla D_{\text{KL}} [\hat{H}_{\text{bare}} : \hat{H}_{\text{eff}}] &= \beta \langle \nabla \hat{H}_{\text{eff}} \rangle_{\text{bare}} - \beta \langle \nabla \hat{H}_{\text{eff}} \rangle_{\text{eff}} \\ &- \int dx P(\hat{H}_{\text{bare}}; x) \nabla \log |\Lambda_{\text{eff}}^{(x)}|. \end{aligned} \quad (\text{S9})$$

In particular, if the eigenbasis of \hat{H}_{imp} does not depend on the coupling constants $\{\theta\}$ of the effective model, then $\nabla_\theta \log |\Lambda_{\text{eff}}^{(x)}| = 0$, and so

$$\nabla_\theta D_{\text{KL}} [\hat{H}_{\text{bare}} : \hat{H}_{\text{eff}}] = \beta \langle \nabla_\theta \hat{H}_{\text{eff}} \rangle_{\text{bare}} - \beta \langle \nabla_\theta \hat{H}_{\text{eff}} \rangle_{\text{eff}}. \quad (\text{S10})$$

Eq. S10 is suitable for GD optimization methods. The optimized effective model is found when the gradient vanishes, $\nabla_\theta D_{\text{KL}} [\hat{H}_{\text{bare}} : \hat{H}_{\text{eff}}] = 0$, which arises when the observables evaluated in bare and effective models match. This constitutes a rigorous derivation for quantum impurity type problems of an ML optimization scheme for effective models based on observables. However, as we have shown, this prescription does not necessarily yield an effective model with the correct low-energy physics. On the other hand, if an effective model is sought that reproduces the value of a particular observable in the bare model, this ML scheme is effective and efficient due to the guaranteed convexity of the optimization landscape.

DETAILS OF NRG CALCULATIONS

In this work, we used Wilson's NRG method [8], formulated in the complete Anders-Schiller basis [9], to calculate the partition functions of Anderson and Kondo models at finite temperature T . Numerical results for the impurity contribution to entropy were obtained by standard thermodynamic NRG [8], while the dynamical t-matrix and local spin-spin correlator observables were obtained using the full density matrix approach [10]. The spectrum of the t-matrix is defined $t(\omega) = -\pi \rho \text{Im} \sum_{\text{kk}'} t_{\text{kk}'}(\omega)$. All parameters are given in units of the conduction electron bandwidth, here set to $D = 1$. Calculations were performed with NRG discretization parameter $\Lambda = 2.5$, retaining $N_s = 3500$ states at each iteration, and exploiting Q and S_z quantum numbers. Interleaved NRG (iNRG) could be used with model ML in principle [11]. We note that for the purposes of model ML, the partition functions need not be calculated exactly: within some given level of approximation applied to both bare and effective models, only the *difference* $\mathcal{Z}_{\text{bare}} - \mathcal{Z}_{\text{eff}}$ needs to be estimated to perform the optimization [12]. Although NRG is used here, the ML methods we describe do not depend on the techniques used to estimate the partition functions or observables.

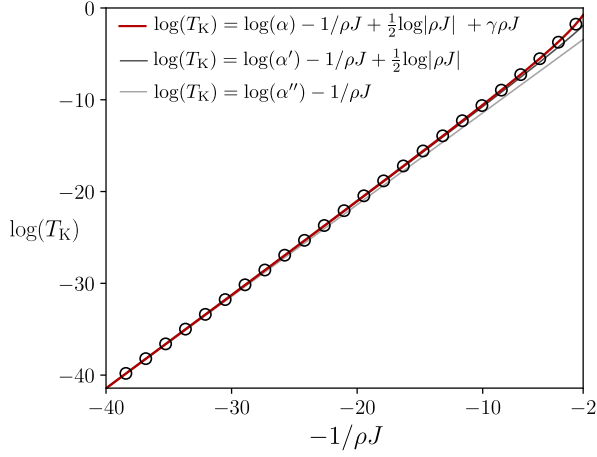


Figure S2. Kondo scale T_K of the pure Kondo model, Eq. 4, as a function of Kondo coupling ρJ , determined from NRG (points), compared with the full analytic result Eq. 5 (red line). $D_K = 1$. The agreement is quantitatively precise over the entire range of ρJ considered. The other lines show the breakdown of lower-order approximations to T_K at larger ρJ .

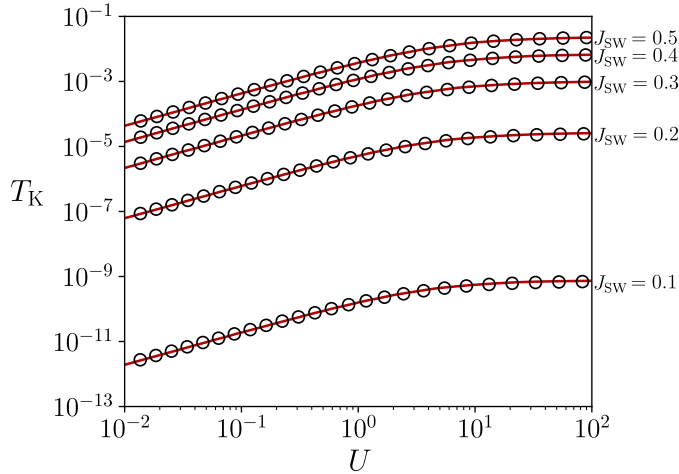


Figure S3. Kondo scale T_K of the (symmetric) Anderson impurity model, Eq. 3, as a function of interaction strength U for various $J_{\text{SW}} = 8V^2/U$, determined from NRG (points), compared with Eq. 6. $D = 1$. Good agreement is seen for all U and J values considered, even in non-perturbative regimes.

KONDO SCALES

All physical observables are universal functions of T/T_K in the scaling limit of the AIM or Kondo models, and so the definition of the Kondo temperature T_K can be chosen somewhat arbitrarily up to an overall con-

stant. In this work, we choose $\alpha = 1.41$ in Eq. 5, so that the conductance half-width-at-half-maximum through an Andersonian dot is precisely at $T = T_K$. As such, this is a natural experimentally-relevant measure. However, for the Anderson / Kondo models, this definition is equivalent to choosing $S_{\text{imp}}(T = T_K) \simeq 0.5$, $t(\omega = T_K, T = 0) \simeq 0.63$, $T_K \chi_{\text{imp}}(T = T_K) \simeq 0.1$, or $T_K = 0.236/\chi_{\text{imp}}(T = 0)$. In practice we use the latter.

In Fig. S2 we confirm that the Kondo scale for a pure Kondo model follows Eq. 5 very precisely up to $J/D_K = 0.9$. This is shown using high-quality NRG calculations, in which we retain $N_s = 6000$ states per iteration, and perform the $\Lambda \rightarrow 1$ extrapolation [13]. Full quantitative agreement requires inclusion of the factor proportional to $\gamma = \pi^2/4$ (note that there is some disagreement/confusion in the literature about this factor, which we definitively pin down here).

In Fig. S3 we confirm the accuracy of Eq. 6 for the Kondo scale of the (symmetric) Anderson model in terms of J_{SW} and U , over the whole range $U/D = 10^{-2}$ to 10^2 , and for $J_{\text{SW}}/D = 0.1, 0.2, 0.3, 0.4, 0.5$.

-
- [1] R. Žitko and J. Bonča, Phys. Rev. B **74**, 045312 (2006).
 - [2] F. D. M. Haldane, Journal of Physics C: Solid State Physics **11**, 5015 (1978).
 - [3] A. N. Rubtsov, V. V. Savkin, and A. I. Lichtenstein, Phys. Rev. B **72**, 035122 (2005).
 - [4] E. Gull, A. J. Millis, A. I. Lichtenstein, A. N. Rubtsov, M. Troyer, and P. Werner, Rev. Mod. Phys. **83**, 349 (2011).
 - [5] P. Werner and A. J. Millis, Phys. Rev. B **74**, 155107 (2006).
 - [6] K. Haule, Phys. Rev. B **75**, 155113 (2007).
 - [7] S. Kullback and R. A. Leibler, Ann. Math. Statist. **22**, 79 (1951).
 - [8] K. G. Wilson, Rev. Mod. Phys. **47**, 773 (1975); R. Bulla, T. A. Costi, and T. Pruschke, Rev. Mod. Phys. **80**, 395 (2008).
 - [9] F. B. Anders and A. Schiller, Phys. Rev. Lett. **95**, 196801 (2005).
 - [10] A. Weichselbaum and J. von Delft, Phys. Rev. Lett. **99**, 076402 (2007).
 - [11] A. K. Mitchell, M. R. Galpin, S. Wilson-Fletcher, D. E. Logan, and R. Bulla, Phys. Rev. B **89**, 121105 (2014); K. M. Stadler, A. K. Mitchell, J. von Delft, and A. Weichselbaum, Phys. Rev. B **93**, 235101 (2016).
 - [12] C. H. Bennett, Journal of Computational Physics **22**, 245 (1976).
 - [13] H. Krishna-Murthy, J. Wilkins, and K. Wilson, Physical Review B **21**, 1003 (1980).